Debris characterization in the super/hypersonic and rarefied wind tunnel MARHy

Nicolas Rembaut [(1)], Romain Joussot [(1)], and Viviana Lago [(1)]

[(1)] CNRS, ICARE, UPR 3021, 1c av. de la Recherche Scientifique, CS 50060, F-45071, Orléans cedex 2, France.

ABSTRACT

This paper presents an experimental investigation to determine the influence of the rarefaction effect on shock shapes around a spherical body. Experiments were carried out in the rarefied and super/hypersonic wind tunnel facility MARHy with three different operating flow conditions and several sphere diameters to cover a large range of Knudsen numbers between the near continuum and the slip regime.

1 INTRODUCTION

Considering the constant increase in the number of artificial satellites and the emergence of CubeSat constellations, the frequency of re-entry to Earth will considerably grow in the future. Indeed, at the end of their activity, these satellites not station-keeping or debris will eventually slow down and leave their orbit, especially those in low orbit due to the presence of atmospheric drag [1]. When they return to Earth, a large part of them will be destroyed in the atmosphere, but 10 to 20% could touch the ground. Therefore, it is essential to be able to determine their trajectory to minimize the risks for human population, but predicting the re-entry of space debris remains an open problem as this is a multi-physical task involving aerodynamic simulations in continuum and rarefied regime, with heat transfer calculations and structural breakup predictions. For this purpose, several codes have been developed by different space agencies such as DAS (NASA), ORSAT (NASA), ORSAT-J (JAXA), DRAMA/ SESAM (ESA), DEBRISK (CNES), DRAPS (China), SCARAB (ESA-HTG Germany), PAMPERO (CNES) [2]. However, numerous uncertainties affect the ability to make accurate the predictions such as the material properties, the unknown initial flight conditions or the invalidated model parameters, specially due to the fact that, debris pass through four successive flow regimes, cited in the order of descent: the free molecular flow regime, the transitional regime, the slip flow regime and the continuous regime. In addition, it is necessary to have a good definition of the boundaries of the flow regimes in order to be able to apply the predominant physical phenomena.

Two main categories define these predictor codes: the object-oriented models and the spacecraft oriented models. The first category uses predefined fragments and assumes a fixed break up altitude regardless the re-entry flight history, which is a great drawback to obtain accurate predictions. On the other hand, spacecraft oriented software include more complex models with an extensive database of materials characteristics and is able to predict fragmentation events and shapes, aerodynamic behavior and heat flux [3]. It is easy to understand that all the parameters and models used to determine the point of impact on Earth of an initial object falling back from space at high-speed space are tainted with uncertainties, and have to be verified and validated. Currently, there is a lack of experimental data to validate the models and geometries characteristics used by these codes, in particular in the rarefied regime flow presenting viscous interaction properties that can change the shapes of the shock, aerodynamic coefficients and surface/gas interaction.

The purpose of this work is to provide experimental databases that could be used to improve the aerodynamic physical models used to determine the possible survivability and the trajectory of space debris. This debris can have any forms that have never been studied under rarefied regime. Nevertheless, many of the debris found on the ground are spherical [4]. As a first approach, we have focused the present work on the experimental study of the aerodynamic properties of spherical debris in Mach 4 supersonic rarefied flows ranging from the transitional to the near continuum regime with slip conditions [5, 6]. This experimental study is carried out in the rarefied hypersonic wind tunnel MARHy, belonging at the ICARE laboratory of the CNRS in Orleans, France. Two Mach 4 nozzles working at different static pressure, 2, 8 and 71 Pa have been used to test spherical objects with four different spherical diameters. This gives us a large enough Knudsen number range to progress from continuous to slip flow regime. A back illuminated CMOS camera was used to visualize the flow field, and a pressure probe was used to measure the total pressure fields around the bodies. The shock wave shape and standoff distance have been determined for each test condition, and have been compared to those predicted by the Billig's empirical equation.

2 EXPERIMENTAL SETUP

This experimental study was carried out with one of the three facilities of the platform FAST: “Facilities for Aerothermodynamics & Supersonic Technologies”. This platform includes a set of three wind tunnels allowing to experimentally simulate the conditions of the different phases of an atmospheric re-entry. For this investigation, we used the MARHy (Hypersonic Rarefied Adaptable Mach) wind tunnel to study the rarefaction effects.

2.1 The MARHy wind tunnel

The MARHy facility, previously known as SR3 [7], is a rarefied supersonic/hypersonic continuous operating wind tunnel. It is one of a set of three wind tunnels that allow to reproduce the conditions of the different atmospheric re-entry's phases. A detailed model of the wind tunnel is shown in Fig. 1. The MARHy wind tunnel consists of a main chamber and a pumping unit. The main chamber is an assembly of three parts (Fig. 1). First of all, there is the settling chamber. It is equipped with a micrometric valve allowing the adjustment of the incoming gas flow rate and allows by its large volume to stabilize the pressure before the nozzle. The nozzle acts as the interface between the settling chamber and the experimental chamber and produces the high speed flow stream. The experimental chamber is 5 m long and has a diameter of 2 m. This large size makes it possible to avoid wall effects and also facilitates the setup of experiments. The experimental chamber is coupled to a diffuser which is connected to the pumping unit to evacuate the gases and to maintain low pressure in the experimental chamber. The pumping unit is composed of 2 primary pumps, 2 intermediate Roots blowers and up to 12 Roots blowers. These ensure the continuous level of the vacuum required for the desired flow density conditions. Depending on the degree of rarefaction required, the number of Roots blowers used can be adjusted.

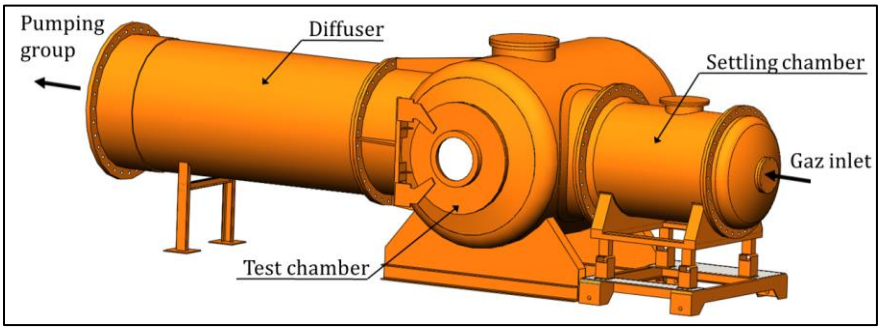

Fig. 1. Scheme of the MARHy wind tunnel without the pumping group.

This facility has a set of nozzles to vary the flow conditions from Mach 0.6 to Mach 30. This set of nozzles of different geometries under optimal operating conditions produces a homogeneous continuous high speed flow stream. The produced flow depends on the nozzle geometry, and the inlet and outlet pressures of the stream. The homogeneous region of the flow has a smaller diameter than the outlet diameter of the nozzle. Due to the rarefaction effects of our conditions, the boundary layer along the divergent part of the nozzle is thickened. In order to obtain reliable results we use only the homogeneous region of the flow, namely the central part, also called the isentropic core. For each nozzle used, it is necessary to take into account the homogeneous flow stream dimensions where the conditions are constant (Mach number, etc.). Consequently, the experimental models are limited in size and depend on the dimensions of the diameter of each nozzle's core.

Tab. 1. Mach 4 flow conditions of the 3 nozzles used.

Stagnation cond.	Flow conditions	Stagnation cond.	Flow conditions	Stagnation cond	Flow conditions
p_0 = 10.797 Pa	p_1 = 71 Pa	p_0 = 1.214 Pa	p_1 = 8.0 Pa	p_0 = 404 Pa	p_1 = 2.7 Pa
T_0 = 293 K	T_1 = 69.76 K	T_0 = 293 K	T_1 = 69.76 K	T_0 = 293 K	T_1 = 69.76 K
ρ_0 = 0.13 kg.m^{-3}	ρ_1 = 3.6 10^{-3} kg.m^{-3}	ρ_0 = 1.4 10^{-2} kg.m^{-3}	ρ_1 = 4.0 10^{-4} kg.m^{-3}	ρ_0 = 4.8 g.m^{-3}	ρ_1 = 1.3 10^{-4} kg.m^{-3}
	μ_1 = 4.77 10^{-6} Pa.s		μ_1 = 4.77 10^{-6} Pa.s		μ_1 = 4.77 10^{-6} Pa.s
	U_1 = 669.61 m.s^{-1}		U_1 = 669.61 m.s^{-1}		U_1 = 669.61 m.s^{-1}
	Ma_1 = 4.0		Ma_1 = 4.0		Ma_1 = 4.0
	λ_1 = 0.012 mm		λ_1 = 0.106 mm		λ_1 = 0.318 mm
	q_m = 2.65 10^{-2} kg.s^{-1}		q_m = 2.98 10^{-3} kg.s^{-1}		q_m = 1.0 10^{-3} kg.s^{-1}

In this study, to determine the influence of the Knudsen number on the shape of the shock wave around a sphere, we built our experimental plan in order to vary the Knudsen number from the continuous regime to the slip flow regime. For this purpose, we chose three nozzles with a Mach number of 4 but with pressures ranging from 71 Pa to 2 Pa. These operating conditions are described more precisely below (Tab. 1). To complete this Knudsen range, 4 spheres of different diameters were selected: 10, 25, 30, and 40 mm. This provides a complete range of Knudsen numbers between the continuous regime and the slip flow regime (Fig. 2). In addition, this distribution gives us two redundant configurations in terms of Knudsen number, but with different freestream pressure and diameters of sphere, allows us to cross-check the data, for one value of Kn.

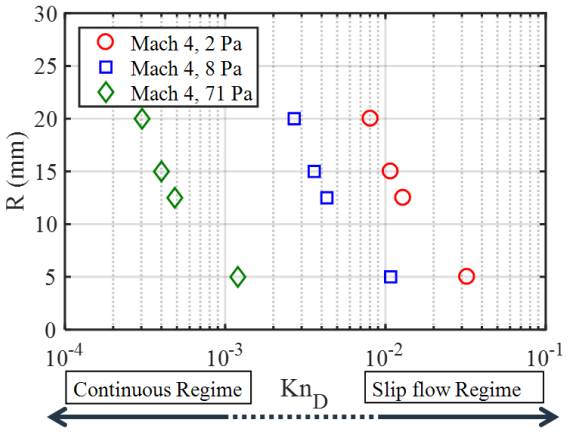

Fig. 2. Flow conditions tested in terms of Knudsen numbers Kn_D and sphere radius R.

2.2 Experimental set up and diagnostics

As presented in Fig. 3, the spherical models are placed at the center of the core flow, aligned with the axis flow. It is important to notice that the flows are produced by a contoured nozzle, meaning that flows are laminar and perfectly homogeneous. Two different diagnostic methods have been used to determine position of the shock around the models: a Pitot probe and the luminescence visualization technique.

The stagnation pressure measurement

The stagnation pressure profiles around the spheres are obtained with a Pitot probe connected to a MKS Baratron capacitance manometer 0-100 Torr connected to a MKS control unit (PDR-C-2C). A 3-axis traversing system, controlled by a computer, ensures the displacement of the Pitot probe with a step resolution on each axis of 0.1 mm ± 0.02 mm on each position.

The Pitot probe is a tube made of stainless steel with a flat-ended cylinder with an external diameter 2.3 mm and an internal diameter of 1.18 mm. In regard to these dimensions and the free-stream flow conditions, it is not necessary to apply viscous or rarefaction corrections to the pressure measurements performed with the Pitot probe. Although, the outer diameter of the Pitot probe is of the same order of magnitude as the pressure gradients of the flow field, many studies related to high speed rarefied flows show that it is possible to capture these phenomena if the spatial resolution of the measurement is sufficiently refined [8] with the minimal value of the vertical displacement step of 1 mm in our conditions. In addition, because of the relatively large size of the Pitot tube compared to the flow phenomena, all measurements are referenced with respect to the center of the Pitot tube.

The flow field visualization

Due to the rarefaction level of the flow operating conditions at 8 and 2 Pa, techniques commonly used such PIV or Schlieren cannot be used to visualize the flow filed around a model. Thus the glow discharge technique is used and it consist to weakly ionize the flow to make it visible. A description of this visualization method can be found in [9]. This technique allows shock waves to be distinguished in low density flows, where other techniques, for instance Schlieren, cannot be applied because of the low level density of the flow. The glow discharge visualization technique consists of polarizing a copper ring or copper plate (Fig. 3) with a negative DC electric power supply to weakly ionize the air flowing around a model in the test chamber.

The diffused light emitted from the flow field is focused on the KURO camera, (2048 x 2048 array), Back-illuminated Scientific CMOS. It is equipped with a 94mm VUV lens and placed behind a fluorine window. This optical configuration gives a resolution of 6.25 pixels/mm. As a result, a variation in density in the flow will result in a variation in the luminous intensity of the flow. Since the shock around the obstacle is denser than the flow, the shock is visualized by the variation in intensity and the resulting light of the ionization as presented in Fig. 4, upper-left panel. Initially we used two polarized copper plates, placed parallel to each other, on both side of the flow in order to ionize it. However, this configuration produced a gradient of ionization and therefore gradient of light intensity from the anode to the cathode. Thus, to improve this technique we used a copper ring in view to obtain a better homogeneous ionization.

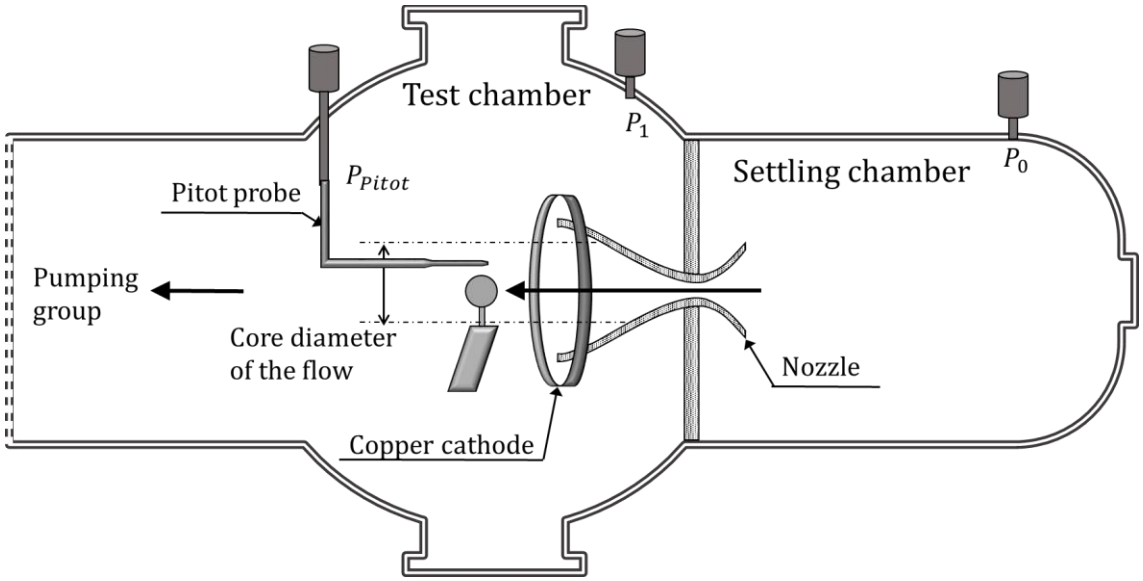

Fig. 3. Schematic view of the experimental setup in the test chamber.

3 RESULTS AND DISCUSSION

The shock wave shape around a spherical body moving in a compressible flow can be described with the empirical expression proposed by Billig [10]:

$$x = R + \Delta - R_c \, cotan^2\theta \left[\left(1 + \frac{z^2 tan^2\theta}{R_c^2}\right)^{1/2} - 1\right], \quad (1)$$

where R is the sphere radius, R_c is the vertex radius of curvature, and Δ is the standoff distance given by the empirical relation proposed by Ambrosio and Wortman [11]. The vertex radius is calculated by the following equation:

$$R_c/R = 1.143 \exp(0.54/(M-1)^{1.2}), \quad (2)$$

and the empirical standoff distance is calculated by the following equation:

$$\Delta/R = 0.143 \exp(3.24/M^2). \quad (3)$$

The shock wave position (*i.e.*, *x* and *z* coordinates in Eq. 1) is a function of the Mach number and does not depend on the rarefaction condition of the flow (*i.e.*, the Knudsen number of the freestream flow). In the case of the continuous flow regime, the empirical relations of Billig [10] and Ambrosio and Wortman [11] (Eqs. 1-3) are known to describe accurately both the shape and the position of the shock wave in front of a sphere (*i.e.*, the standoff distance). In the present study, the set of 12 experimental conditions (Fig. 2) allows to analyze the deviation from the empirical formulations in case of increasing Knudsen number, with experimental cases in the slip flow regime.

3.1 Determination of shock wave shapes

For the experimental cases with freestream pressure of 2.7 Pa and 8.0 Pa, the shock wave around each sphere was analyzed using visualization technique and from the image recorded by the CMOS camera. For each case, a series of 200 raw images were recorded and the average image was calculated (Fig. 4, upper-left panel). Then the background image was subtracted to the average field of raw images to enhance its contrast (Fig. 4, upper-right panel). To detect the shock wave around the model, the gradient function of the Matlab software was used (Fig. 4, bottom-left panel). This mathematical function allows to considerably improve the visualization of the shock wave in comparison to the average field of raw images. Finally, both the sphere and the shock wave position were detected using an edge detection function from the Matlab software (Fig. 4, bottom-right panel).

Figure 4 shows that the shock wave is detached from the model since a standoff distance of a few mm is clearly visible on each image. By measuring this distance for each experimental case, the expected deviation of Δ from the empirical formulation (Eq. 3) of Ambrosio and Wortman [11] can be seen. The shock wave position estimated from the edge detection is compared to the shock wave's shape estimated at Mach 4 with the empirical relation (Eq. 1) of Billig [10].

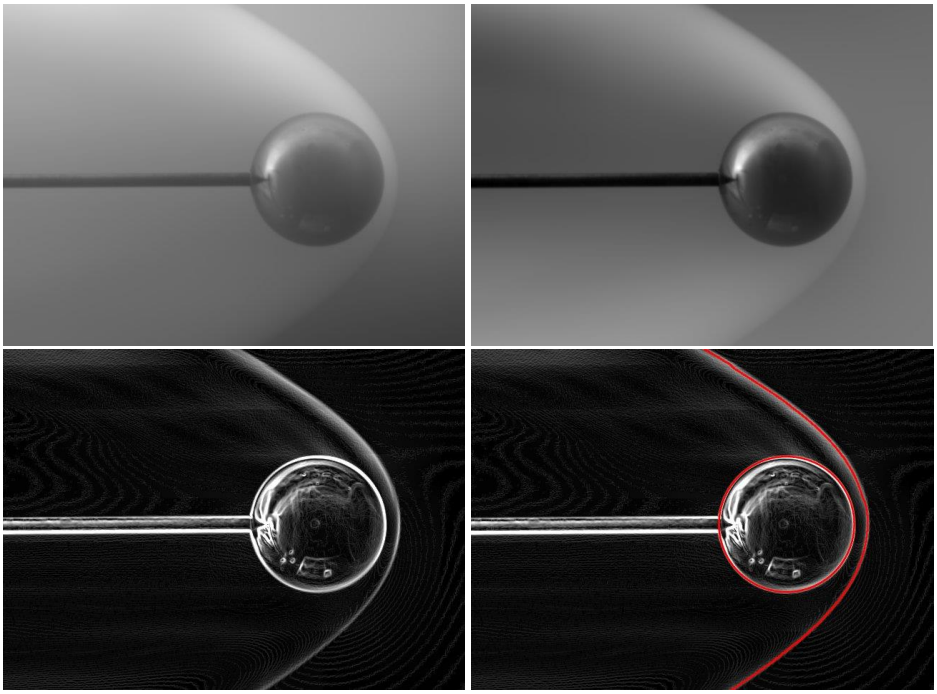

Fig. 4. Images of the flow field around a 30 mm-sphere (Mach 4 – 8.0 Pa): average field of the raw images (upper-left panel), average field with background subtraction (upper-right panel), Matlab's gradient function applied (bottom-left panel), and Matlab's edge detection function applied (bottom-right panel).

Figure 5 shows that the shock wave position predicted with the empirical relation of Billig [10] fails to reproduce the actual shock wave position obtained during the experiments in rarefied flow condition typical of the slip flow regime. A gap is clearly visible between the two curves in Fig. 5, left panel. Moreover, Fig. 5, right panel, clearly demonstrates that the standoff distance increases with the rarefaction of the flow, independently of the radius of sphere (R = 12.5 mm in Fig. 5). One can observe that the shock wave is more detached from the model for the case with the lowest freestream pressure (*i.e.*, with the highest Knudsen number). This result is independent of the fact that for same experimental conditions the standoff distance Δ increases with the radius of sphere as expressed by the equation Δ/R.

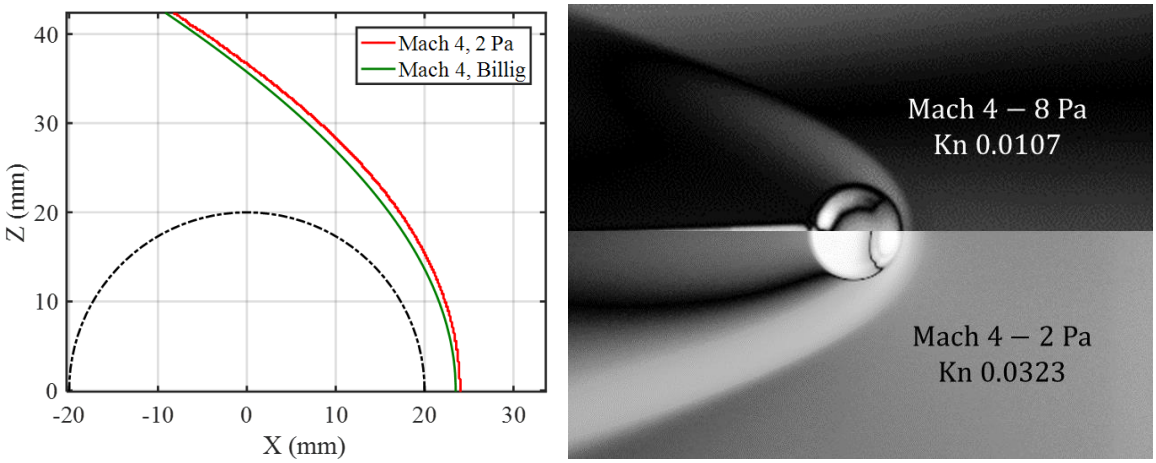

Fig. 5. Shock wave positions: comparison of the experimental shock wave position obtained at Mach 4 – 2.7 Pa with the position given by the empirical relation of Billig (Eq. 1) around a 40 mm-diameter sphere (left panel), and comparison of the standoff distance obtained with a 5 mm-diameter sphere in a Mach 4 – 8.0 Pa flow (top) and in a Mach 4 – 2.7 Pa flow (bottom).

For the highest freestream pressure tested at Mach 4 (71 Pa), visualization of the flow field around the sphere by the glow-discharge technique cannot be employed due to the high background pressure [12]. In this case, the shock wave's shape above the sphere was detected by probing the flow field with a Pitot tube. For each diameter of sphere, several vertical profiles (*i.e.*, along *z*-axis) were realized at different longitudinal positions (*i.e.*, along *x*-axis). By detecting the minimum gradient of each vertical Pitot profile, the shock wave position can be detected accurately at a given *x*-position [12]. However, this method does not allow to obtain the shock wave position in front of the sphere, and the shock standoff distance could not be measured directly for the Mach 4 – 71 Pa flow conditions.

Figure 6 shows the comparison between the shock wave position obtained with the Pitot profile and the position given by the empirical formulation of Billig (Eq. 1) in considering a flow at Mach 4. One can observe that a very good agreement is obtained between experimental data points and the empirical curve. From this result, we can assume that the experimental shape of the shock wave obtained with a Mach 4 – 71 Pa flow can be described by the empirical equation of Billig [10], irrespective of the diameter of the sphere. The empirical equation used to calculate the Δ/R ratio (Eq. 3) can therefore be used to estimate the standoff distance for the Mach 4 – 71 Pa flow condition. For the smallest value of the sphere diameter (D = 10 mm), the Knudsen number based on the freestream conditions (Tab. 1) and the sphere diameter D is 1.2×10^{-3}, which corresponds to a value close to the threshold of the slip flow regime.

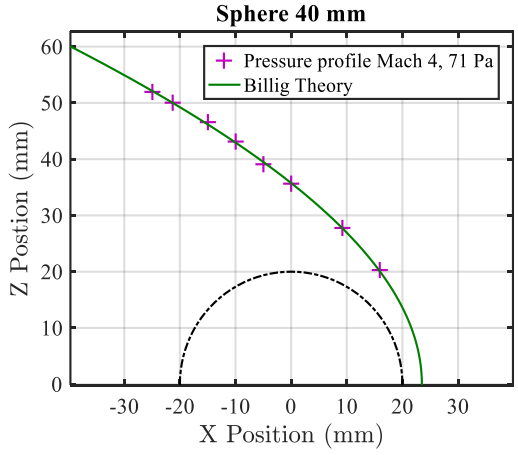

Fig. 6. Shock wave position around the 40 mm-diameter sphere for the Mach 4 – 71 Pa flow condition. Data points correspond to the shock wave position estimated from the Pitot profiles.

3.2 Analysis of the standoff distance behavior

In the case of the Mach 4 – 2.7 Pa and Mach 4 – 8.0 Pa flow conditions (*i.e.*, the most rarefied flow conditions), the standoff distances were determined from the analyses of the images recorded with the CMOS camera (Fig. 4). The experimental conditions for each of the four spherical diameters corresponding to the slip flow regime with $Kn_D > 2\times10^{-3}$. For the Mach 4 – 71 Pa flow condition, the empirical equation of Ambrosio and Wortman (Eq. 3) was used to calculate the value of Δ.

Figure 7 shows the standoff distances according to the sphere radius for the three experimental flow conditions. One can observe that three different sets of data points are clearly visible, meaning that the empirical equation of Ambrosio and Wortman [11] fails to evaluate accurately the standoff distance in the case of flow conditions typical of the slip flow regime, and will probably fail to estimate Δ for the more rarefied flow regimes (*i.e.*, transition and free molecular flow regimes). In addition, Fig. 7 shows that the standoff distance increases linearly with the radius of the sphere, irrespective of the rarefaction level of the flow (for the slip flow regime).

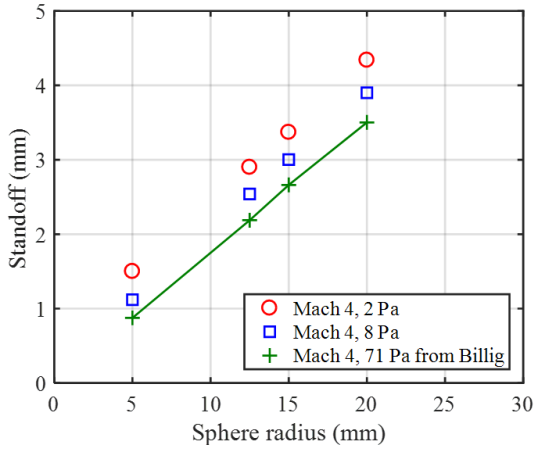

Fig. 7. Standoff distance according to the sphere radius for the 3 freestream pressures tested at Mach 4. Data point for the 71 Pa case correspond to the values estimated with the empirical formulation of Billig (Eq. 1).

The rarefaction level can be represented by the Knudsen number Kn, which was calculated for each experimental conditions with respect to the sphere diameter (Fig. 2) and the flow conditions of the present study (Tab. 1). Figure 8 shows the variation of the Δ/R ratio as a function of the Knudsen number Kn_D (based on the sphere diameter).

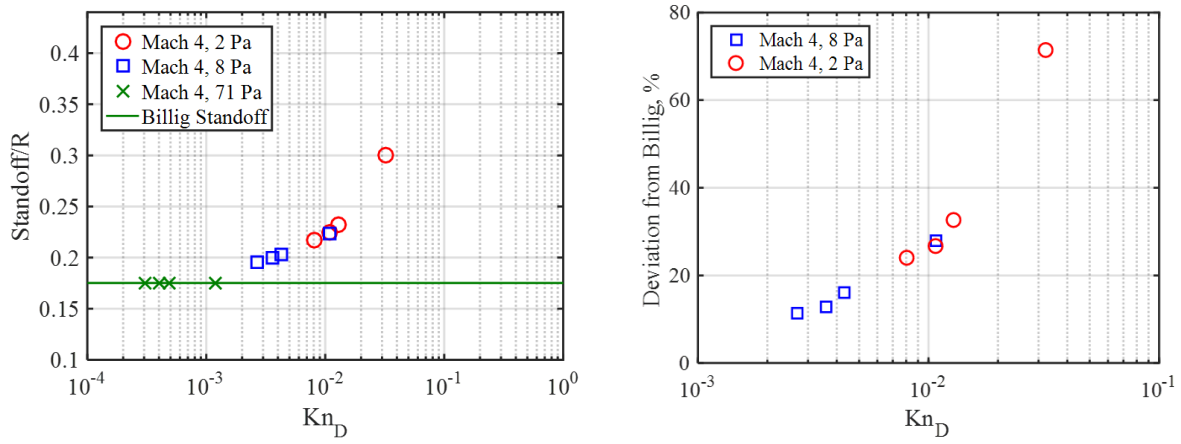

Fig. 8. Ratio of the standoff distance with the sphere radius according to the Knudsen number (left panel), and relative difference between the experimental standoff distance and the value calculated with the empirical equation (Eq. 3) according to the Knudsen number (right panel) .

One can observe a sharp increase of the values Δ/R when the Knudsen number becomes greater than 6×10^{-3}, thus showing that the standoff distance predicted by the Billig's equation are largely under estimated when the flow is of the slip regime. Indeed, as presented in Fig. 8 b, the deviation between the experimental standoff and the one predicted by the Billig's equation can reach 70 % for a Knudsen number of 0.03. The deviation ranges is still between 10 and 20 % for Knudsen values which, according to the theory, correspond to the continuous regime. It is important to note that the range of the Knudsen number values, according the experimental test cases presented in this work, correspond to the beginning of slip regime, which suggest that this gap should grow when approaching the free molecular regime, before reaching a threshold value.

We are now interested in the curve of the shock wave, without taking into account the standoff distance. The Billig's equation was used to calculate new curve of the shock using as an input the standoff distance corresponding to the experimental one, and then have been compared to the experimental shock shape. Result are presented in Fig. 9 for a Mach 4 - 2 Pa experimental condition and a sphere diameter of 40 mm. As observed, there is a good agreement between the experimental shock shape and the new calculated one that shows that despite the change of the regime flow, from continuous to slip regime, the shape of the shock seems quite not affected. So the increase of the Knudsen number slightly influences the shock shape but significantly influences the standoff distance.

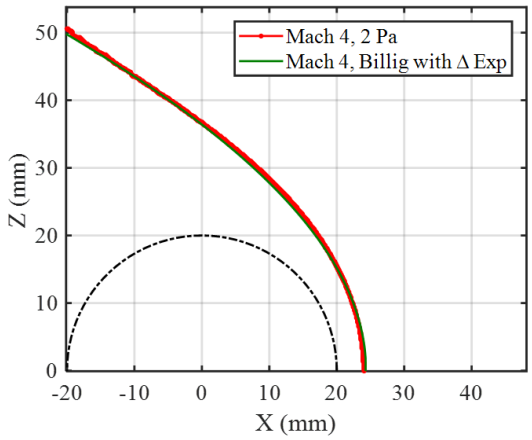

Fig. 9. Comparison of the experimental shock wave position at Mach 4 – 2.7 Pa (red curve) and the position calculated with the empirical equation of Billig and shifted of the actual standoff value determined from the experiment (green curve).

Finally, in view of the results discussed above, the Knudsen number has a direct impact on the global position of the shock. Indeed, as the detachment increases with the number of Knudsen starting from 10^{-3}, it has the effect of detaching the shock wave from the body. Figure 10 shows the impact of detachment on the global shock wave shape for different degrees of rarefaction as a percentage deviation from Billig's standoff shown on the right in Fig. 8.

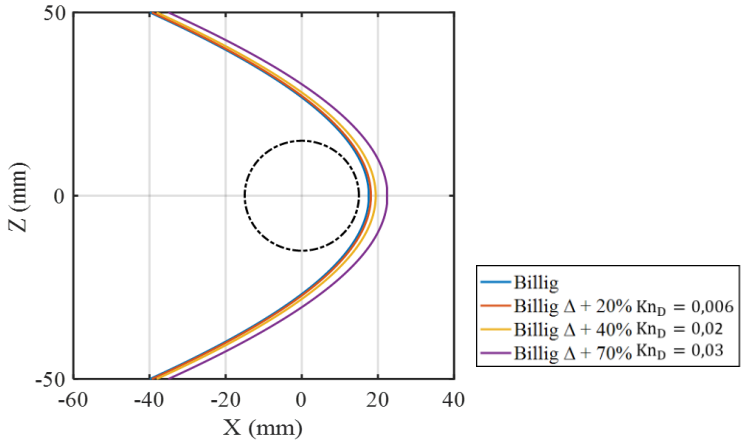

Fig. 10. Shock wave positions for several rarefaction levels, at Mach 4.

4 CONCLUSIONS

The present experimental investigation focuses on a better understanding of the influence of rarefaction effects on the re-entry trajectories of space debris. We therefore conducted our experimental investigation at Mach 4 flow, to analyse how low pressure modifies shock properties around spherical models. Experiments have been carried out with the MARHy super/hypersonic rarefied wind tunnel, successively equipped with three different nozzles generating a flow at Mach 4 with static pressures of 71Pa, 8Pa and 2Pa. Different sphere diameters were chosen to obtain Knudsen number ranging from continuous to slip flow regime. We determined coordinates of the shock wave curve and measured the detachment for a range of Knudsen numbers. The present results demonstrate that the standoff distance increases with the Knudsen number. Consequently, the standoff distance does not only depend on the Mach number as expressed by Ambrosio and Wortman [11] but also on the Knudsen number. However, the shape of the shock wave expressed by Billig [10], seems to remain similar.

The next objective of this study is to establish a relationship that would describe shock detachment in terms of rarefaction and Mach number. For this purpose, other nozzles will be used to produce flows at similar static pressure and similar Knudsen number but different Mach number. Future works will focus more on complex shapes such as cubes or hollow cylinders. Currently, a 2-axis aerodynamic balance is under development, which will eventually allow us to study the aerodynamic forces applied to complex objects in a rarefied regime.

5 ACKNOWLEDGEMENTS

Nicolas Rembaut’s Ph.D. fellowship is funded by the Région Centre-Val de Loire. This work was supported by the French National Research Agency (ANR) as part of the “Investments d’Avenir” Programme (LabEx CAPRYSSES; ANR-11-LABX-0006-01).

6 REFERENCES

1. ESA, "Space Environment Report Latest". Technical Note GEN-DB-LOG-00239-OPS-GR. 2018.
2. Prevereaud, Y., Vérant, J. L., Moschetta, J. M., Sourgen, F., and Blanchard, M. "Debris aerodynamic interactions during uncontrolled atmospheric reentry." AIAA Atmospheric Flight Mechanics Conference. 2012.
3. Koppenwallner, Georg, et al. "Scarab-a multi-disciplinary code for destruction analysis of space-craft during re-entry." Fifth European Symposium on Aerothermodynamics for Space Vehicles. Vol. 563. 2005.
4. Prevereaud, Y. "Contribution à la modélisation de la rentrée atmosphérique des débris spatiaux. " Diss. Institut Supérieur de l’Aéronautique et de l’Espace (ISAE), 2014.
5. Coumar, S., and Lago V. "Influence of Mach number and static pressure on plasma flow control of supersonic and rarefied flows around a sharp flat plate." Experiments in Fluids, 58 (6): 74, 2017.
6. Laurence, S. J., Parziale, N. J., and Deiterding, R. “Dynamical Separation of Spherical Bodies in Supersonic Flow”, Journal of Fluid Mechanics, 713:159–82, 2012.
7. Allègre, J. The SR3 low density wind-tunnel. Facility capabilities and research development. In 28th Joint Propulsion Conference and Exhibit, July 06-08, Nashville (TN), U.S.A., AIAA Paper No. 92–3972, 1992.
8. Allègre, J., and C. Bisch. "Angle of attack and leading edge effects on the flow about a flat plate at Mach number 18." AIAA Journal 6.5 848-852, 1968.
9. Fisher, S.S. and Bharathan, D. Glow-discharge flow visualization in low-density free jets. Journal of Spacecraft and Rockets, Vol. 10, No. 10, pp. 658-662, 1973.
10. Billig, F. S. Shock-wave shapes around spherical-and cylindrical-nosed bodies. Journal of Spacecraft and Rockets, Vol. 4, No. 6, pp. 822-823, 1967.
11. Ambrosio, A. and Wortman, A. Stagnation point shock detachment distance for flow around spheres and cylinders. ARS Journal, Vol. 32, No. 2, pp. 281-281, 1962.
12. Joussot R., et al. Quantification of the effect of surface heating on shock wave modification by a plasma actuator in a low density supersonic flow over a flat plate. Experiments in Fluids, Vol. 56, No. 5, p. 102, 2015.